Electronic Supplementary Material (ESI) for Materials Chemistry Frontiers.

Engineering raspberry-like $CuCo_2S_4$@ZnS hollow particles encapsulated by reduced graphene oxide for hybrid supercapacitor

Bahareh Ameri, Akbar Mohammadi Zardkhoshoui*, and Saied Saeed Hosseiny Davarani*

Department of Chemistry, Shahid Beheshti University, G. C., 1983963113, Evin, Tehran, Iran.

Corresponding authors: *Tel: +98 21 22431661; Fax: +98 21 22431661; E-mail: ss-hosseiny@sbu.ac.ir (S.S.H. Davarani); and mohammadi.bahadoran@gmail.com (A. Mohammadi Zardkhoshoui)

Supporting Information

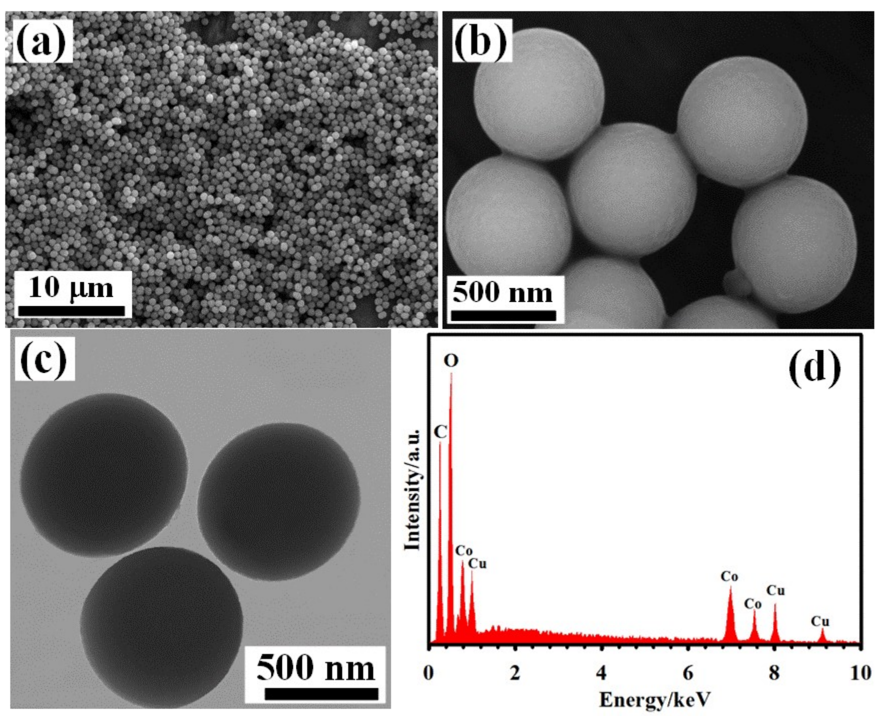

Fig S1 (a, b) FE-SEM images of the CC-GSSs. (c) TEM image of the CC-GSSs. (d) EDX pattern of the CC-GSSs.

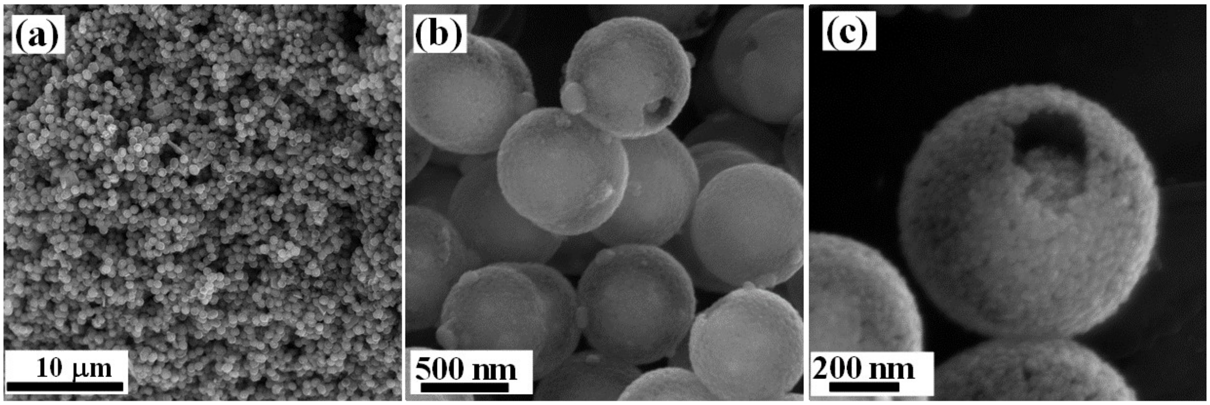

Fig S2 (a-c) FE-SEM images of the CCS-HSs.

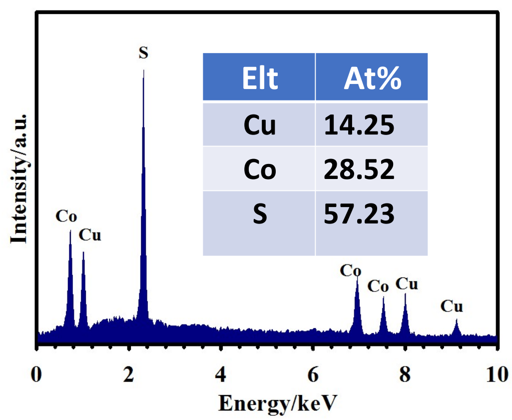

Fig S3 EDX pattern of the CCS-HSs.

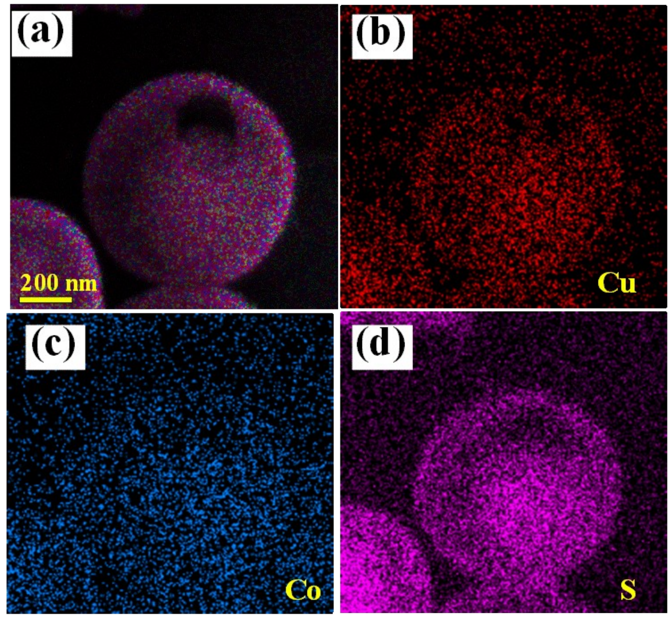

Fig S4 FE-SEM mapping images of the CCS-HSs.

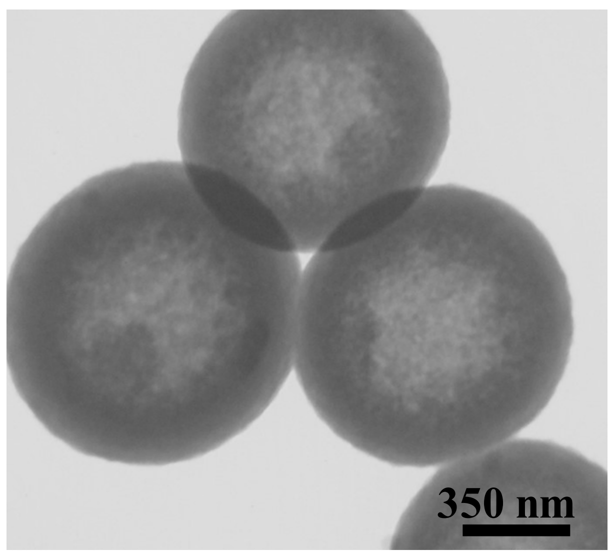

Fig S5 TEM image of the CCS-HSs.

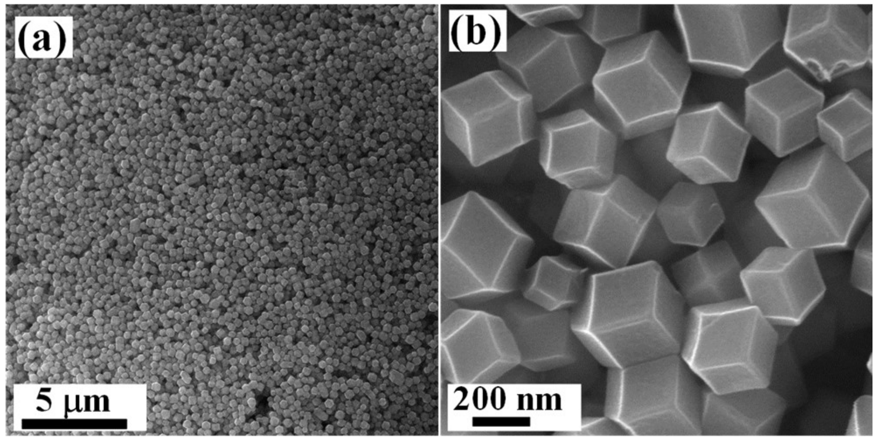

Fig S6 (a, b) FE-SEM images of the ZIF-8.

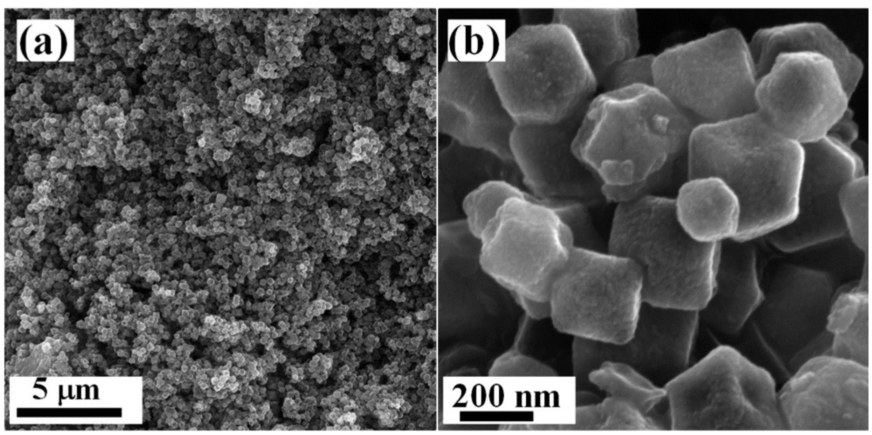

Fig S7 (a, b) FE-SEM images of the ZnS.

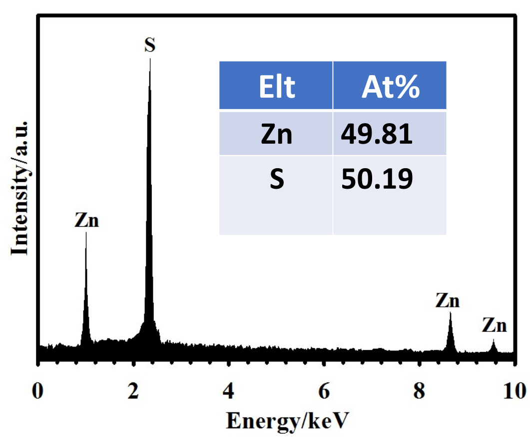

Fig S8 EDX pattern of the ZnS.

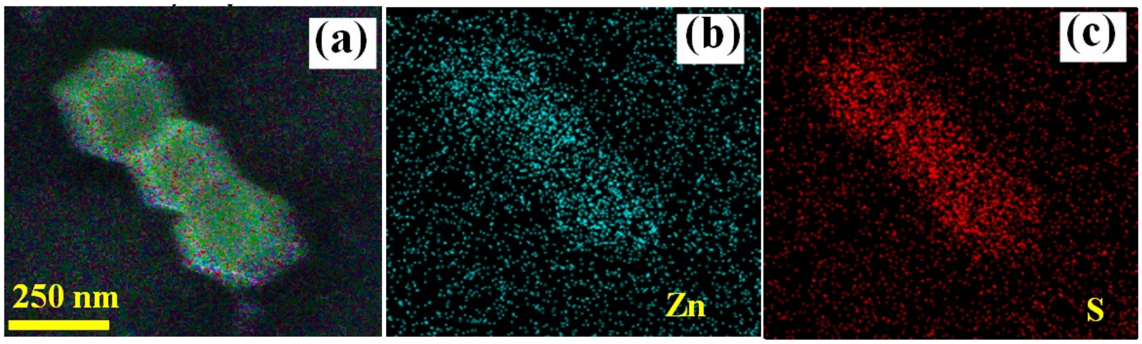

Fig S9 FE-SEM mapping images of the ZnS.

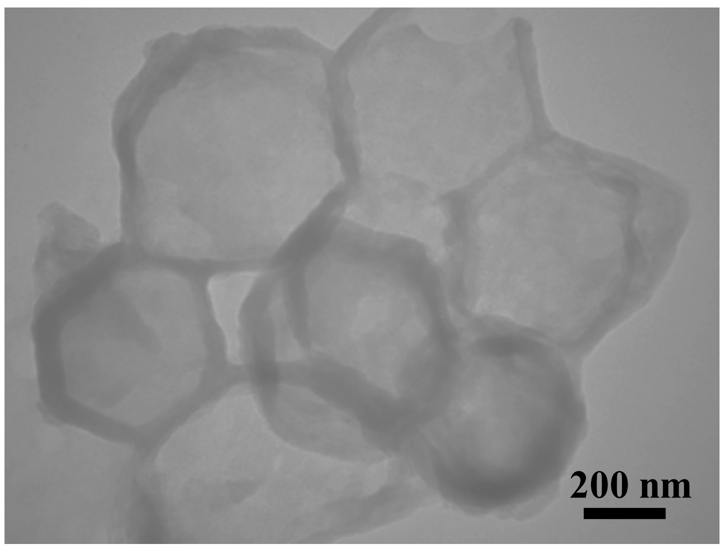

Fig S10 TEM image of the ZnS.

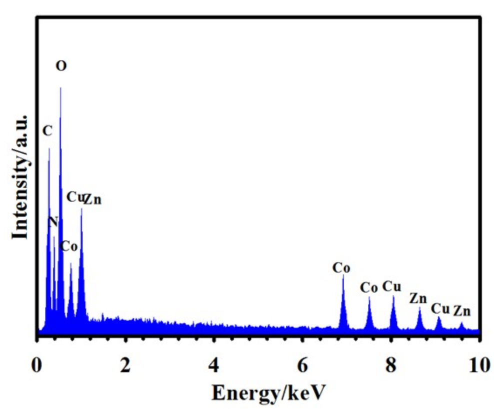

Fig S11 EDX pattern of the CC-G@ZIF-8.

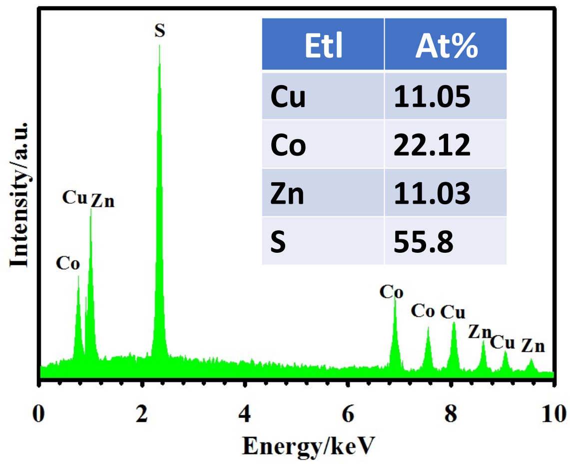

Fig S12 EDX pattern of the RCCS-ZSH8 sample.

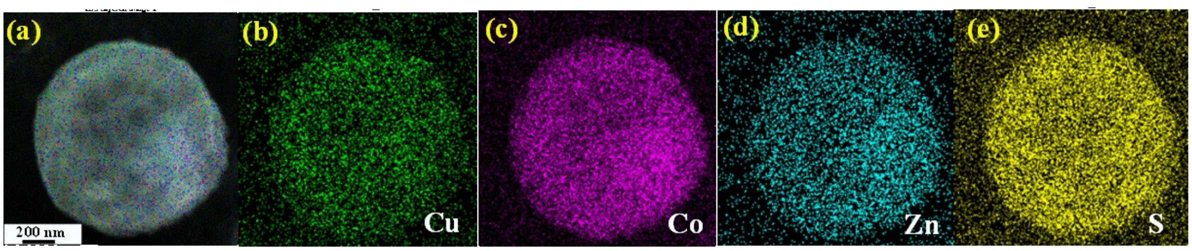

Fig S13 FE-SEM mapping images of the RCCS-ZSH8 sample.

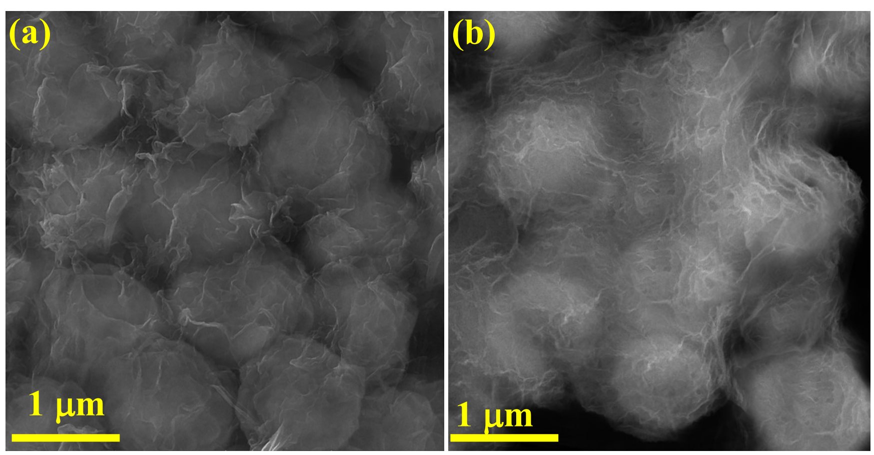

Fig S14 (a) FE-SEM images of the RCCS-ZSH8-rGO1 sample. (b) FE-SEM images of the RCCS-ZSH8-rGO3 sample.

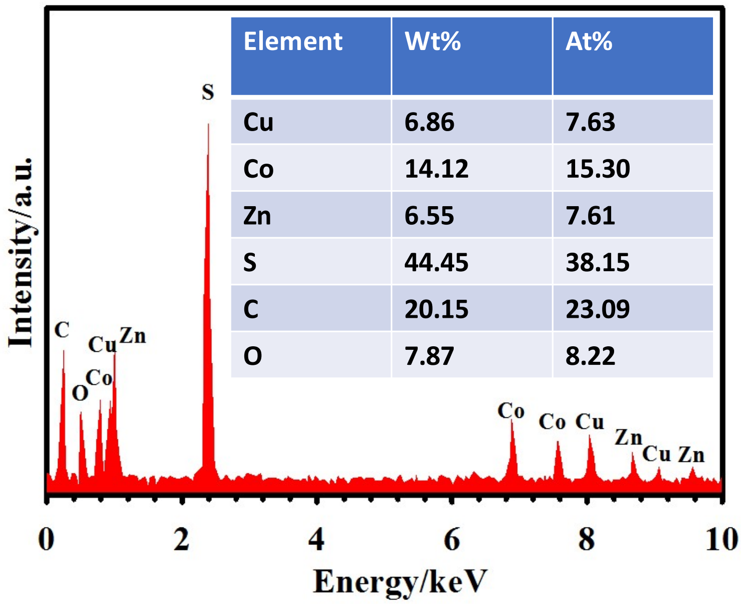

Fig S15 EDX pattern of the RCCS-ZSH8-rGO2 sample.

The EDX analysis of the RCCS-ZSH8-rGO2 reveals the weight percentage of Cu, Co, Zn, S, C, and O elements in the RCCS-ZSH8-rGO2 are about 6.86%, 14.12%, 6.55%, 44.45%, 20.15%, and 7.87%. Accordingly, the contents of $CuCo_2S_4$, ZnS, and rGO in the RCCS-ZSH8-rGO2 are estimated to be 56.54 wt%, 15.44 wt%, and 28.02 wt%, respectively. Based on the weight of Cu (6.86%), Co (14.12%), and S (44.45%) elements, the content of the $CuCo_2S_4$ in the RCCS-ZSH8-rGO2 is calculated as about 56.54 wt% [6.86% + 14.12% + (44.45/5%)×4%], the content of the ZnS in the RCCS-ZSH8-rGO2 is calculated as about 15.44 wt% [(6.55% + (44.45/5%))], and content of the rGO in the RCCS-ZSH8-rGO2 is calculated as about 28.02 wt% [100% - (56.54%+15.44%)]. Hence, the weight ratio of $CuCo_2S_4$, ZnS, and rGO in the RCCS-ZSH-rGO2 can be calculated, as approximately 1.83:0.50:0.90.

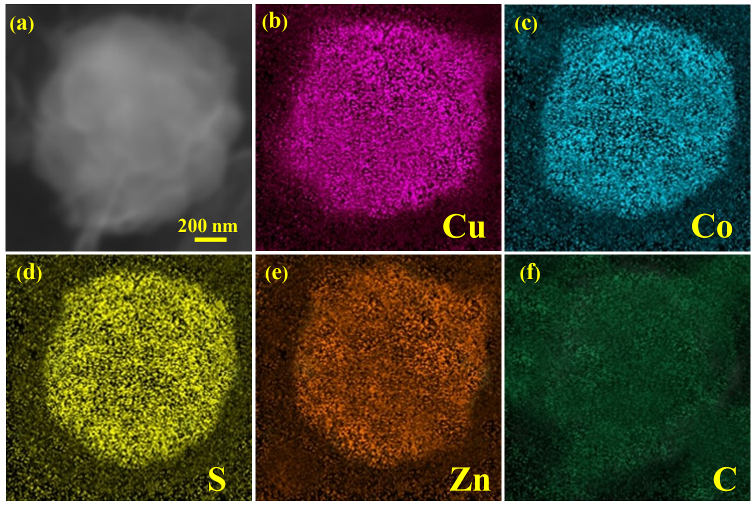

Fig S16 FE-SEM mapping images of the RCCS-ZSH8-rGO2 sample.

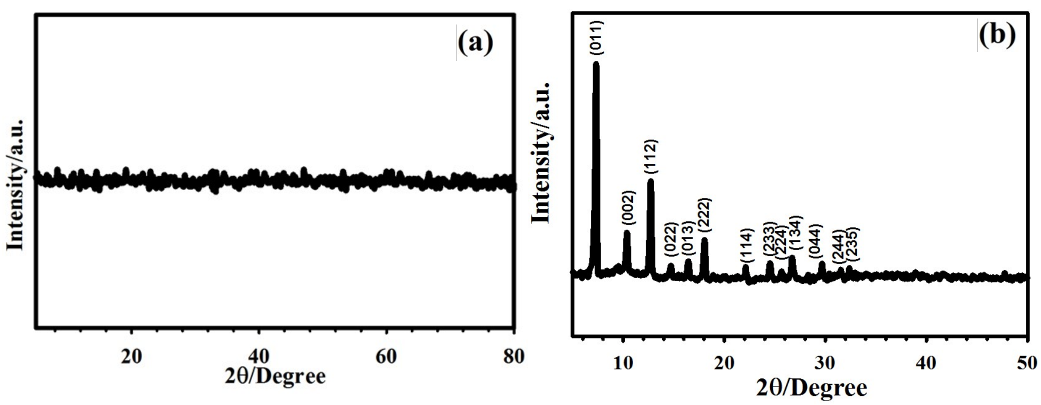

Fig S17 (a) XRD pattern of the CC-GSSs. (b) XRD pattern of the CC-G@ZIF-8.

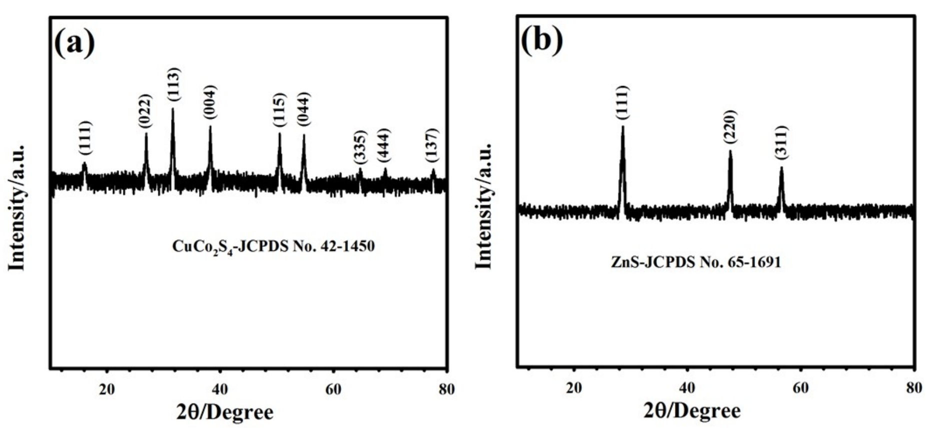

Fig S18 (a) XRD pattern of the CCS-HSs. (b) XRD pattern of the ZnS.

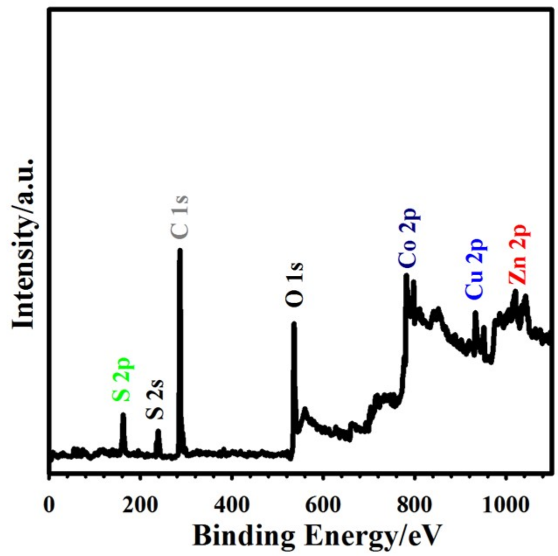

Fig S19 XPS survey of the RCCS-ZSH8-rGO2 sample.

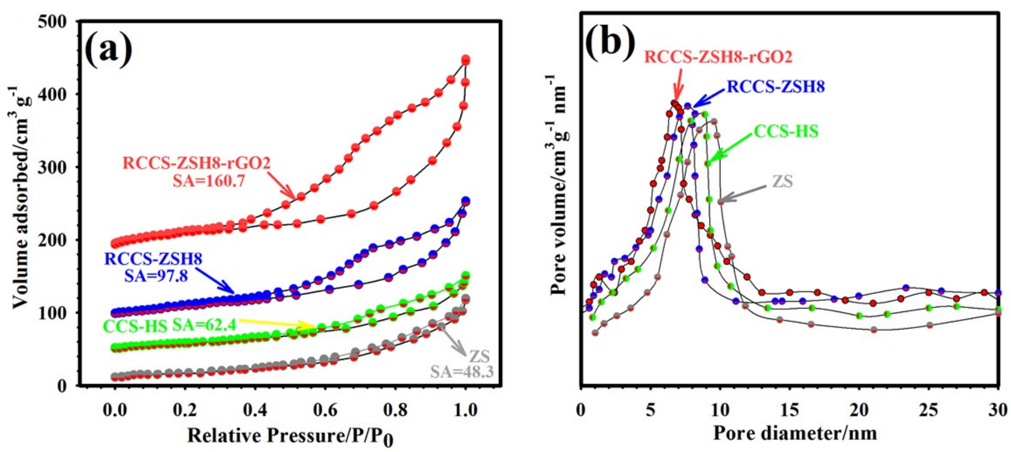

Fig S20 (a) BET plots of the RCCS-ZSH8-rGO2, RCCS-ZSH8, CCS-HS, and ZnS samples. (b) BJH curves of the RCCS-ZSH8-rGO2, RCCS-ZSH8, CCS-HS, and ZnS samples.

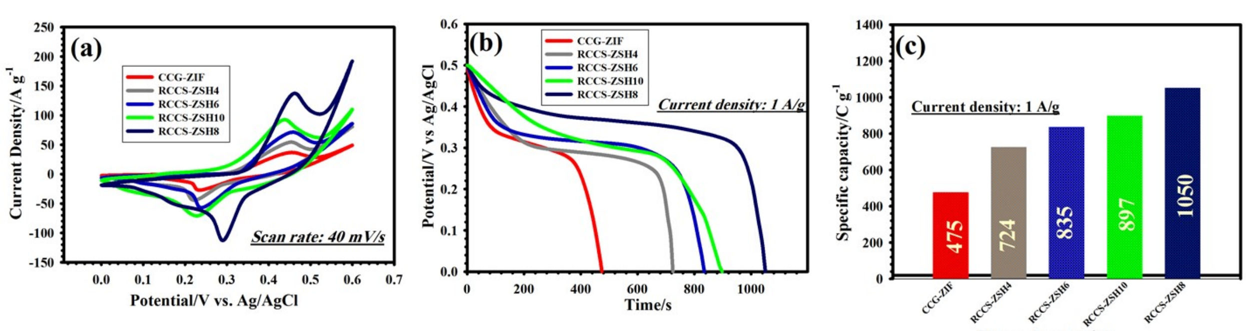

Fig S21 (a) CV curves of the CCG-ZIF, RCCS-ZSH4, RCCS-ZSH6, RCCS-ZSH8, and RCCS-ZSH10 electrodes at 40 mV s^{-1}. (b) Discharge curves of the CCG-ZIF, RCCS-ZSH4, RCCS-ZSH6, RCCS-ZSH8, and RCCS-ZSH10 electrodes at 1 A g^{-1}. (c) Specific capacities of the CCG-ZIF, RCCS-ZSH4, RCCS-ZSH6, RCCS-ZSH8, and RCCS-ZSH10 electrodes at 1 A g^{-1}.

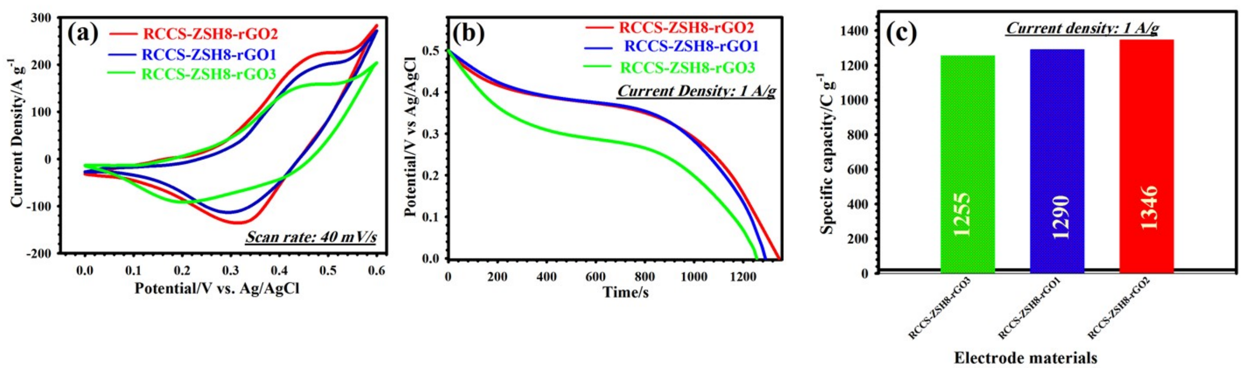

Fig S22 (a) CV curves of the RCCS-ZSH8-rGO1, RCCS-ZSH8-rGO2, and RCCS-ZSH8-rGO3 electrodes at 40 mV s^{-1}. (b) Discharge curves of the RCCS-ZSH8-rGO1, RCCS-ZSH8-rGO2, and RCCS-ZSH8-rGO3 electrodes at 1 A g^{-1}. (c) Specific capacities of the RCCS-ZSH8-rGO1, RCCS-ZSH8-rGO2, and RCCS-ZSH8-rGO3 electrodes at 1 A g^{-1}.

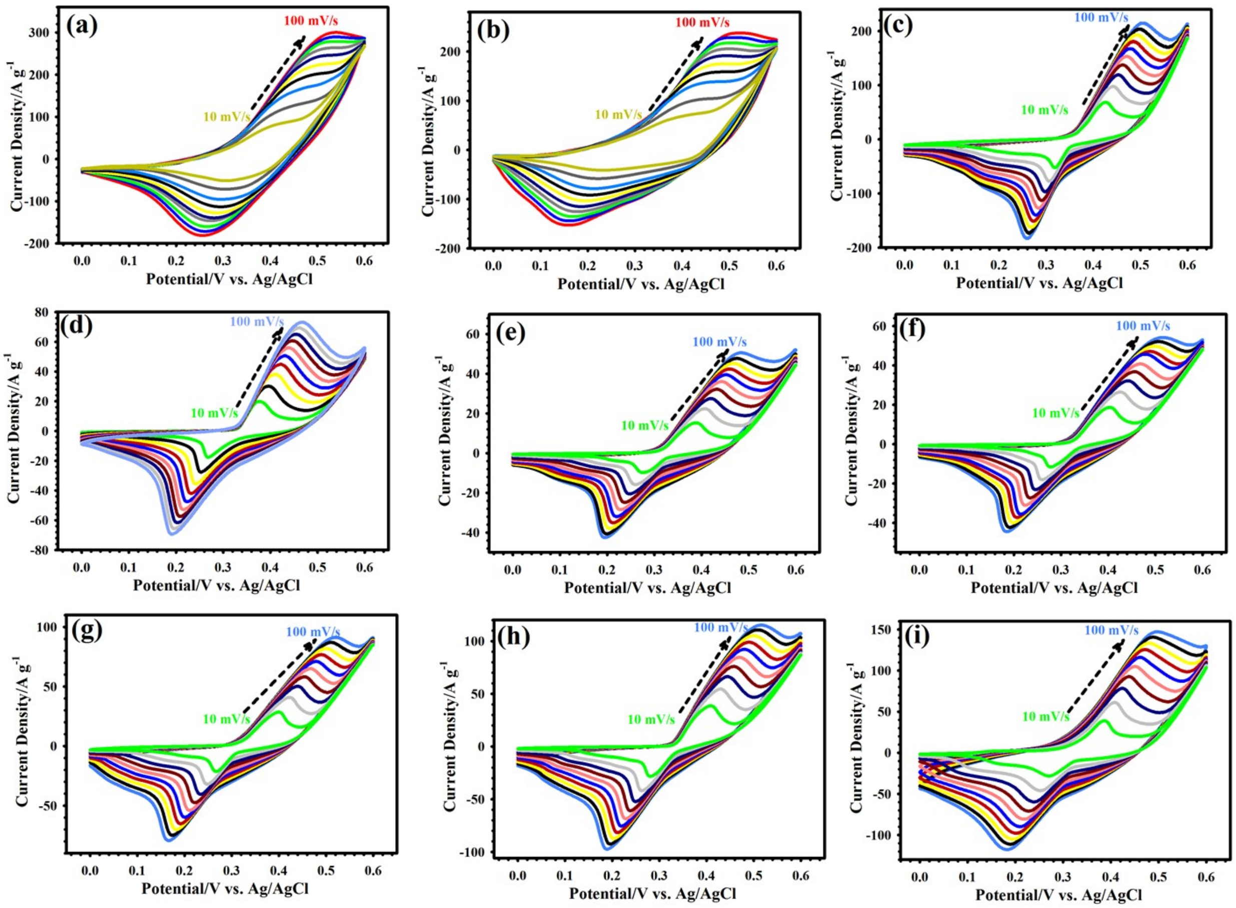

Fig S23 (a) CV curves of the RCCS-ZSH8-rGO1 electrode at various scan rates from 10 to 100 mV s^{-1}. (b) CV curves of the RCCS-ZSH8-rGO3 electrode at various scan rates from 10 to 100 mV s^{-1}. (c) CV curves of the RCCS-ZSH8 electrode at various scan rates from 10 to 100 mV s^{-1}. (d) CV curves of the CCS-HS electrode at various scan rates from 10 to 100 mV s^{-1}. (e) CV curves of the ZS electrode at various scan rates from 10 to 100 mV s^{-1}. (f) CV curves of the CC-G@ZIF electrode at various scan rates from 10 to 100 mV s^{-1}. (g) CV curves of the RCCS-ZSH4 electrode at various scan rates from 10 to 100 mV s^{-1}. (h) CV curves of the RCCS-ZSH6 electrode at various scan rates from 10 to 100 mV s^{-1}. (i) CV curves of the RCCS-ZSH10 electrode at various scan rates from 10 to 100 mV s^{-1}.

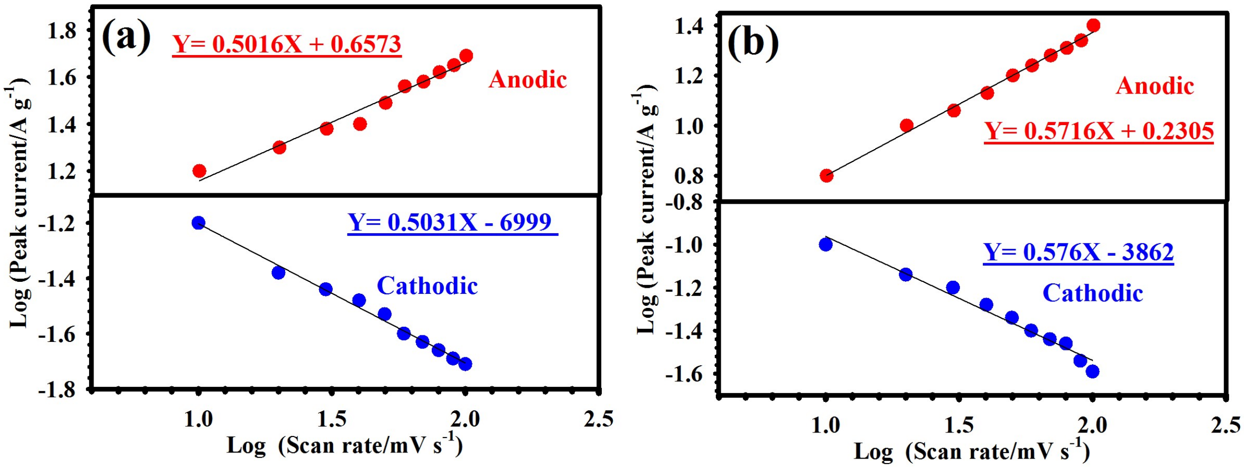

Fig S24 (a) Linear relation between the plot of the Logarithm (i) versus Logarithm (υ) of the CCS-HS electrode. (b) Linear relation between the plot of the Logarithm (i) versus Logarithm (υ) of the ZS electrode.

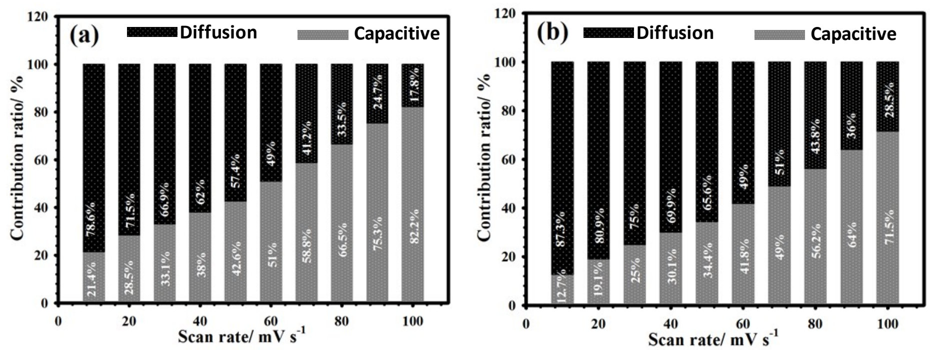

Fig S25 (a) Diffusion and capacitive contributions of the RCCS-ZSH8-rGO2 electrode at different scan rates. (b) Diffusion and capacitive contributions of the RCCS-ZSH8 electrode at different scan rates

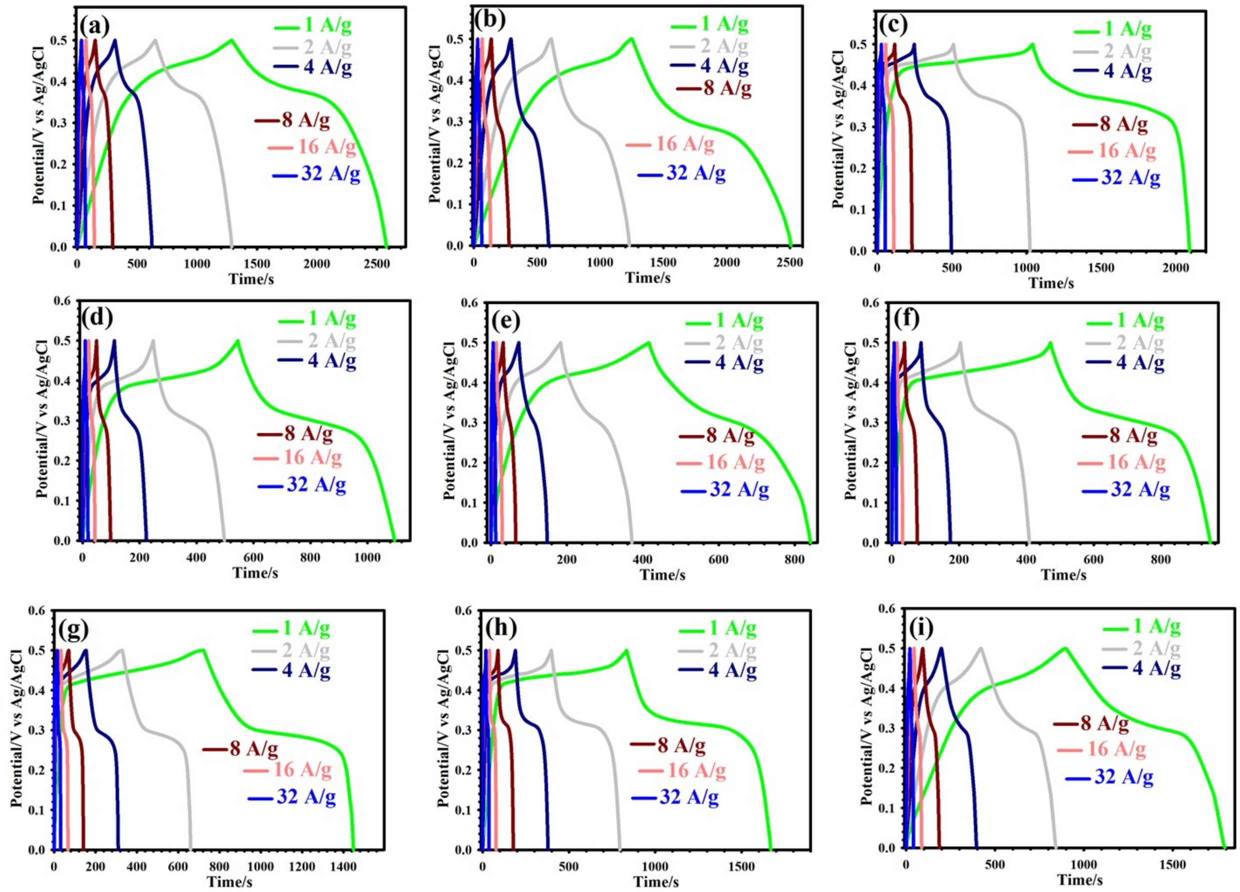

Fig S26 (a) GCD curves of the RCCS-ZSH8-rGO1 electrode at various current densities from 1 to 32 A g^{-1}. (b) GCD curves of the RCCS-ZSH8-rGO3 electrode at various current densities from 1 to 32 A g^{-1}. (c) GCD curves of the RCCS-ZSH8 electrode at various current densities from 1 to 32 A g^{-1}. (d) GCD curves of the CCS-HS electrode at various current densities from 1 to 32 A g^{-1}. (e) GCD curves of the ZS electrode at various current densities from 1 to 32 A g^{-1}. (f) GCD curves of the CCG-ZIF electrode at various current densities from 1 to 32 A g^{-1}. (g) GCD curves of the RCCS-ZSH4 electrode at various current densities from 1 to 32 A g^{-1}. (h) GCD curves of the RCCS-ZSH6 electrode at various current densities from 1 to 32 A g^{-1}. (i) GCD curves of the RCCS-ZSH10 electrode at various current densities from 1 to 32 A g^{-1}.

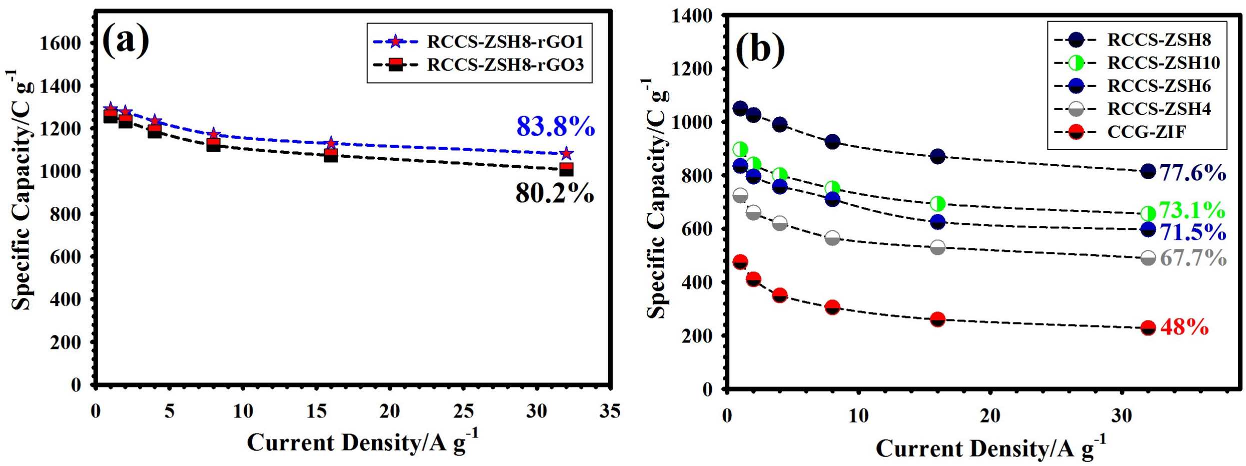

Fig S27 (a) Rate capability of the RCCS-ZSHS8-rGO1 and RCCS-ZSH8-rGO3. (b) Rate capability of the CCG-ZIF, RCCS-ZSH4, RCCS-ZSH6, RCCS-ZSH8, and RCCS-ZSH10.

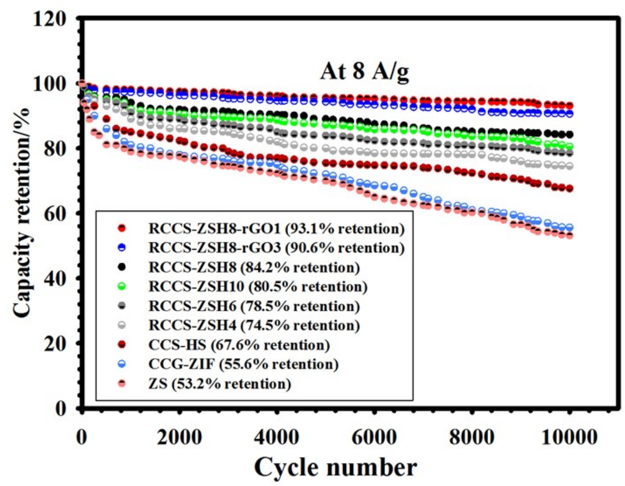

Fig S28 Longevity of the RCCS-ZSH8-rGO1, RCCS-ZSH8-rGO3, RCCS-ZSH8, RCCS-ZSH10, RCCS-ZSH6, RCCS-ZSH4, CCS-SH, CCG-ZIF, ZS electrodes at 8 A g^{-1}.

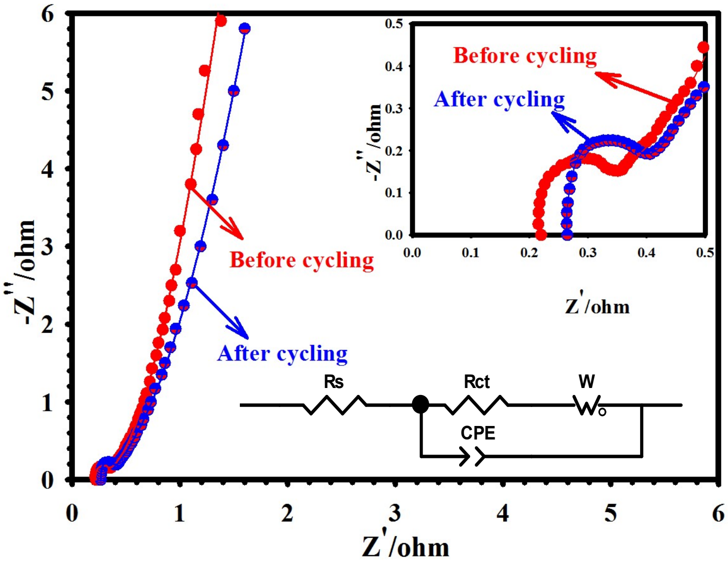

Fig S29 Nyquist plots of the RCCS-ZSH8-rGO2 before and after 10000 cycles.

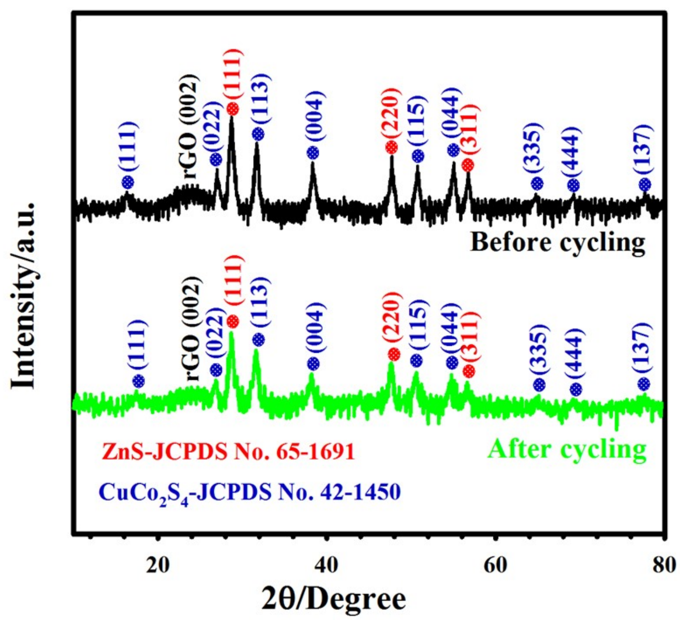

Fig S30 XRD pattern of the RCCS-ZSH8-rGO2 sample before and after 10000 cycles.

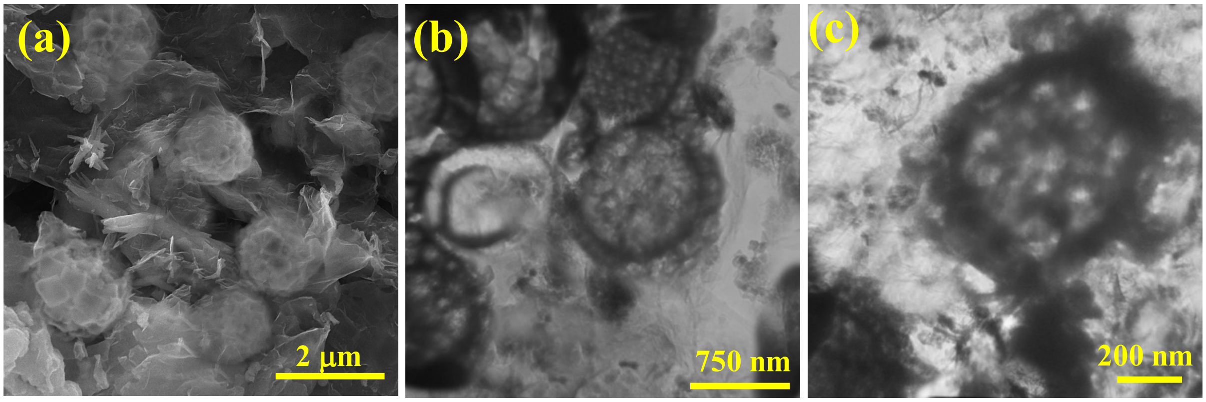

Fig S31 (a) FE-SEM image of the RCCS-ZSH8-rGO2 sample after 10000 cycles. (b, c) TEM images of the RCCS-ZSH8-rGO sample after 10000 cycles.

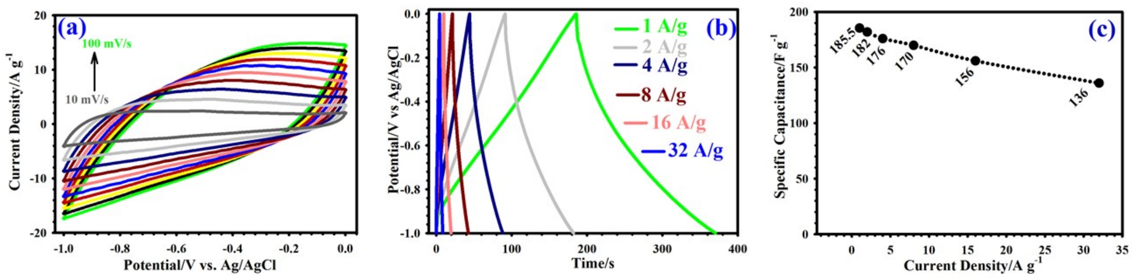

Fig S32 (a) CV plots of the AC at various scan rates from 10 to 100 mV s^{-1}. (b) GCD plots of the AC at various current densities from 1 to 32 A g^{-1}. (c) Rate capability of the AC electrode.

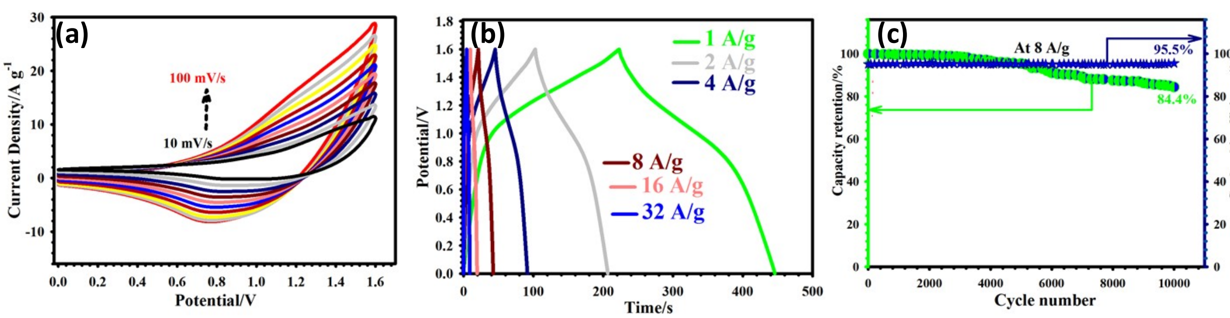

Fig S33 (a) CV plots of the RCCS-ZSH8//AC device at various scan rates from 10 to 100 mV s^{-1}. (b) GCD plots of the RCCS-ZSH8//AC device at various current densities from 1 to 32 A g^{-1}. (c) Durability and coulombic efficiency of the RCCS-ZSH8//AC at 8 A g^{-1}

Table S1 Comparison of the performance of the RCCS-ZSH8-rGO2 with other previously reported materials.

Composition	**Capacity (C/g)**	**Cycles, retention**	**Rate capability**	**ED (Wh kg^{-1})**	**Reference**
FSNCS	**559.3 at 1 A g^{-1}**	**50000, 88.9%**	**68.6% at 20 A g^{-1}**	**28.8**	**1**
NiCoMn-S-1.5	**657.7 at 1 A g^{-1}**	**50000, 90%**	**51.61% at 50 A g^{-1}**	**36.3**	**2**
Ni-Co-sulfide	**603 at 1 A g^{-1}**	**8000, 91.3%**	**67.4% at 15 A g^{-1}**	**45.35**	**3**
Co_3S_4@PPy	**723 at 1 A g^{-1}**	**1000, 98.6%**	**41.77% at 10 A g^{-1}**	**30.2**	**4**
Co_3S_4/g-C_3N_4-10	**415 at 0.5 A g^{-1}**	**5000, 75.6%**	**54.5% at 10 A g^{-1}**	**37.7**	**5**
NiCoMn-S	**661 at 1 A g^{-1}**	**1000, 86.45%**	**66.56% at 50 A g^{-1}**	**42.1**	**6**
Ni–Co–S-0.5/NC	**543.9 at 1 A g^{-1}**	**5000, 90.5%**	**67.3% at 20 A g^{-1}**	**39.6**	**7**
NiCo2S4/NGF	**558 at 1 A g^{-1}**	**6000, 92.6%**	**55.5% at 20 A g^{-1}**	**36.8**	**8**
RCCS-ZSH8-rGO	**1346 at 1 A g^{-1}**	**10000, 95.4 (3 E)**	**86.6% at 32 A g^{-1}**	**66.6**	**This study**

References

1 J. Wang, J. Wang, G. Zhu, H. Xu, X. Zhang, Y. Zhao, J. Zhang, K. Jiang and A. Yu, Simple controllable foam structure $NiCo_2S_4$ for high-performance hybrid supercapacitors, *J Energy Storage* 2022, **46**, 103907.

2 J. Zhang, C. Li, M. Fan, T. Ma, H. Chen and H. Wang, Two-dimensional nanosheets constituted trimetal Ni-Co-Mn sulfide nanoflower-like structure for high-performance hybrid supercapacitors, *Appl. Surf. Sci*. 2021, **565**, 150482.

3 Y. Deng, X. Wang, Z. Wang, X. Wang, Z. Li, L. Wang, C. Zhou, D. Chen and Y. Luo, Yolk–Shell Structured Nickel Cobalt Sulfide and Carbon Nanotube Composite for High-Performance Hybrid Supercapacitors, *Energy Fuels* 2021, **35**, 5342–5351.

4 W. Huo, X. Zhang, X. Liu, H. Liu, Y. Zhu, Y. Zhang, J. Ji, F. Dong and Y. Zhang, Construction of advanced 3D Co_3S_4@PPy nanowire anchored on nickel foam for high-performance electrochemical energy storage, *Electrochim. Acta* 2020, **334**, 135635.

5 W. Li, Y. Li, C. Yang, Q. Ma, K. Tao and L. Han, Fabrication of 2D/2D nanosheet heterostructures of ZIF-derived Co_3S_4 and g-C_3N_4 for asymmetric supercapacitors with superior cycling stability, *Dalton Trans* 2020, **49**, 14017-14029.

6 J. Cao, Y. Hu, Y. Zhu, H. Cao, M. Fan, C. Huang, K. Shu, M. He and H. C. Chen, Synthesis of mesoporous nickel-cobalt-manganese sulfides as electroactive materials for hybrid supercapacitors, *Chem. Eng. J* 2021, **405**, 126928.

7 M. Yi, C. Zhang, C. Cao, C. Xu, B. Sa, D. Cai and H. Zhan, MOF-Derived Hybrid Hollow Submicrospheres of Nitrogen-Doped Carbon-Encapsulated Bimetallic Ni–Co–S Nanoparticles for Supercapacitors and Lithium Ion Batteries, *Inorg. Chem*. 2019, **58**, 3916–3924.

8 Y. Chen, T. Liu, L. Zhang and J. Y, $NiCo_2S_4$ Nanotubes Anchored 3D Nitrogen-Doped Graphene Framework as Electrode Material with Enhanced Performance for Asymmetric Supercapacitors, *ACS Sustainable Chem. Eng*. 2019, **7**, 11157–11165.